Investigation of the Formation of MCM-41 by Electron Spin−Echo Envelope Modulation Spectroscopy

Jingyan Zhang,[†] Patrick J. Carl,[†] Herbert Zimmermann,[‡] and Daniella Goldfarb*,[†]

Department of Chemical Physics, Weizmann Institute of Science, Rehovot, 76100, Israel, and Max-Planck Institute for Medical Research, D-6900 Heidelberg, Germany

Received: December 18, 2001

The electron spin−echo envelope modulation (ESEEM) technique was used to investigate the formation mechanism of the mesoporous material MCM-41. The spin-probes 4-(*N*,*N*-dimethyl-*N*-hexadecyl)ammonium-2,2,6,6,-tetramethyl piperidine-oxyl iodide (CAT16) and 5-doxyl stearic acid (5DSA) were introduced into the surfactant (cetyltrimethylammonium bromide, CTAB) solution in minute amounts followed by the addition of a base and a silica source to initiate the reaction. The reaction was then quenched at different times by rapid insertion into liquid nitrogen. The preservation of the micellar structure upon freezing was proved by a series of ESEEM measurements carried out on 5DSA in CTAB solutions of various concentrations, which showed that the ^{14}N modulation depth was sensitive to the transition from spherical to cylindrical micelles. Variations in the immediate environment of the spin-probes occurring during the room temperature formation of MCM-41 were followed by tracing the ^2H modulation depth $k(^2H)$ induced by α-d_2-CTAB molecules and D_2O. For both spin-probes, $k(^2H)$ of α-d_2-CTAB decreased throughout the reaction, whereas $k(^2H)$ of D_2O showed a small increase. In all cases, the time evolution of $k(^2H)$ revealed two stages: one that lasted for the first ∼12 min, during which most changes have occurred, followed by a second, longer one with mild changes. The reduction of $k(^2H)$ of α-d_2-CTAB in the case of 5DSA was assigned to its displacement toward the organic core, driven by charge repulsion between negatively charged silicate oligomers at the interface and the negative polar head of 5DSA. Considering the different position of the nitroxide spin label in CAT16 and 5DSA with respect to the α-position in the CTAB molecules, the decrease in $k(^2H)$ for CAT16 was attributed to an upward displacement, and a protrusion into the soft silica layer, driven by steric consideration and charge attraction. The slight increase in $k(^2H)$ due to D_2O shows that the silica layer formed in the room temperature synthesis is water rich such that the density of water and OH groups in the vicinity of the spin-probes increases. The majority of the water, however, is easily removed just by filtering the solid formed and drying at room temperature. Finally, evidence for the rearrangement of surfactant molecules and the increase of the aggregate size during the first stage of the reaction was obtained from changes in the echo decay time.

Introduction

The concept of using large molecular assemblies of organic molecules as templates for the preparation of porous oxides, introduced by Mobil researchers in the synthesis of the silica based M41S materials,[1] has led to the proliferation of strategies for the synthesis of ordered mesoporous materials. These employ a variety of organic templates and inorganic precursors that generate materials with a wide range of structures and properties.[2,3] While extensive research efforts have been directed toward the synthesis of new and highly stable materials and their characterization, relatively little investigations have been devoted to the detailed elucidation of the formation mechanism of the various synthesis routes. Such mechanistic studies are hampered by two main reasons: the first is the limited availability of physical methods and probes that allow *in situ* investigations of the process and the second is the difficulties to determine intermolecular interactions and distances in materials that are not crystalline. The intermolecular interactions within the organic aggregates and between the surfactant molecules and the inorganic precursors play a major role in the formation mechanism as they comprise the driving force for the assembly of the final structure.

So far, the most extensively studied systems have been those prepared with charged templates, specifically MCM-41, which has an hexagonal arrangement of pores. In this particular case there is a general understanding of its formation mechanism on a macroscopic level. The mechanism agrees, in principle, with the first formulation of the liquid crystal templating mechanism postulated in the original Mobil team report[1] where they envisioned two possible pathways. In the first, a liquid crystalline phase preexists, the silicate species adsorb at its interface and condense there to generate the silica wall. In the second, a liquid crystalline phase is first induced by the interaction of the surfactant preexisting micelles and the silicate species, followed by the silicate condensation to form the silica wall. The synergism of the organic molecular assemblies and the inorganic precursors to form structures with long range order have been nicely demonstrated by Firouzi et al.,[4,5] who showed that under conditions of low reactivity of silicate species, it is possible to stabilize lyotropic silicate-surfactant liquid crystals. In this system, the specific association between the silicate oligomers and the surfactant leads to the liquid crystalline phase formation.

[†] Department of Chemical Physics.
[‡] Max-Planck Institute for Medical Research.

10.1021/jp014564g CCC: $22.00
Published on Web 05/02/2002

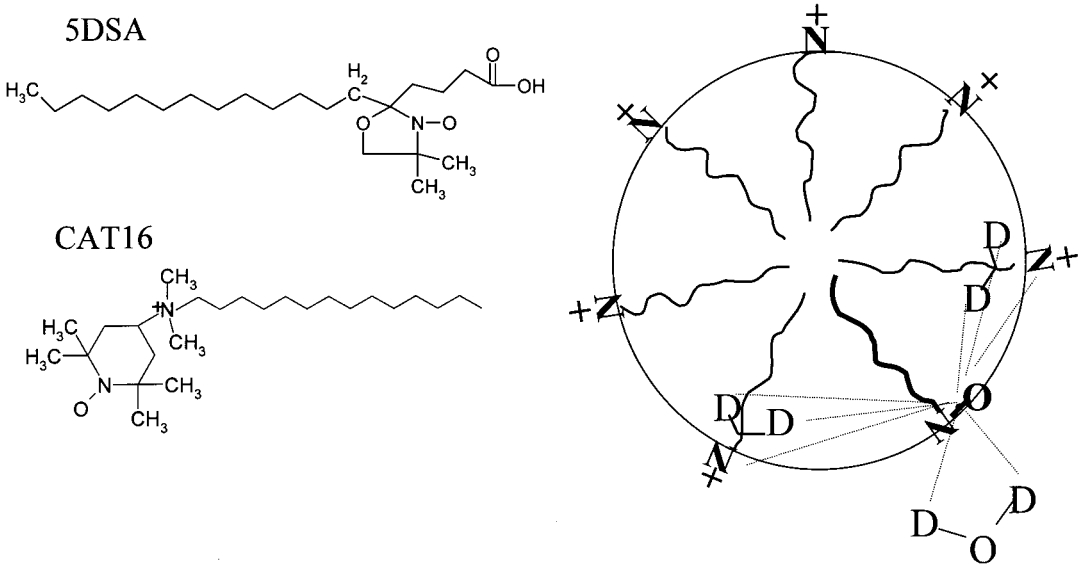

Figure 1. The spin-probes used in this work and a schematic drawing of the a micelle with a spin probe. The dotted lines indicate the interactions that can be detected by ESEEM measurements.

For the charged template systems the following three essential principles were pointed out by Monnier et al.:[6] (i) multidentate binding of silicate oligomers, (ii) preferred polymerization of silicates at the surfactant-silicate interface, and (iii) charge density matching across the interface. For (i) to occur it is assumed that anionic exchange between the surfactant anions and the silicate anions takes place. This, however, has been recently questioned by Zana et al.[7] and Sicard et al.,[8] who showed through fluorescence measurements that only a small fraction of the micelle-bound bromide ions are exchanged with silicate ions. Consequently, they suggested that the most important step in the process is the formation of prepolymers of silicates which interact with the surfactant, leading finally to the formation of a solid organized silica/surfactant complex.

In situ X-ray diffraction (XRD) measurements, using a synchrotron beam, revealed two stages in the formation of MCM-41: the long range order is completed within 3 min and from then on only silica condensation occurs.[9,10] *In situ* IR measurements carried out at high temperatures showed that the ordering of the surfactant molecules increases during the reaction.[11] The formation of MCM-41 under acidic conditions, at the air−water interface, was examined by grazing incident synchrotron radiation diffraction.[12,13] Again, two steps were identified: the first is referred to as an induction period during which ordering of the silicate and surfactant molecules at the interface occurs, and at the end of this stage a diffraction pattern is developed. This is then followed by a rapid growth of a layered structure. This model was also applied to bulk reactions and a kinetic model for the induction period was built.[14] In this case the experimental data fit well the model which is based on exclusive anion association with the micelle surface under acidic conditions. In *in situ* EPR measurements, the changes in the motional and ordering characteristic of spin-probes mixed into the reaction mixture were followed through line shape analysis.[15−17] Those experiments that were carried out with tetraethyl-orthosilicon (TEOS)[15,16] also showed two clear stages: a fast one (∼12 min) attributed to the formation of a long range ordered silicate-surfactant mesophase and a slower one (>1 h), which is devoted primarily to the completion of the silicate polymerization. Other EPR measurements carried out on MCM-41, prepared with sodium silicate,[17] which slows the reaction, lead to a model where the initial phase is a disordered precipitate, consisting of a mixture of spherical micelles and silicate anions. This phase is then gradually depleted due to silicate migration to form the hexagonal phase.[17] In this model, silica-stabilized micelles lengthen at the expense of less stable ones. Clusters of rodlike micelles were observed at the early stage (∼3 min) of the synthesis of MCM-41 by cryo-TEM.[18]

In this work we sought further insight into the formation mechanism of MCM-41, in particular at the early stages of the reaction when the interaction between silicate anions and the surfactant assemblies takes place. We examined the changes occurring in the packing and immediate environment of the surfactant molecules during the room temperature formation of MCM-41 using spin-probes and electron spin−echo envelope modulation (ESEEM) spectroscopy. This technique is particularly useful for the measurement of weak superhyperfine interactions of an unpaired electron with nearby nuclei.[19,20] In these experiments an electron-spin−echo is generated by a specific pulse sequence and the echo decay is monitored. When the unpaired electron experiences a weak hyperfine interaction with nearby nuclei, the echo decay is modulated with the corresponding Larmor frequencies and the modulation depth is proportional to the electron-nuclear distance and the number of interacting nuclei. Kevan and co-workers have extensively applied ESEEM methods to study a variety of photoinization and charge separation problems in micellar and vesicle systems.[21−23] In addition, they have determined the location of nitroxide spin-probes in micelles by following the interaction of the nitroxide group with specifically deuterated surfactant molecules, and investigated the structural effects of additives on the micellar systems.[24,25] Here we followed their approach and used the spin-probes 4-(*N*,*N*-dimethyl-*N*-hexadecyl)ammonium-2,2,6,6,-tetramethyl piperidine-oxyl, iodide (CAT16), and 5-doxyl stearic acid (5DSA), which have structural features similar to those of the surfactant molecules (see Figure 1). Minute amounts of the spin-probes were added to the reaction mixture and the reaction was quenched to liquid N_2 temperatures at different reaction times. It has already been reported that minute amounts of CAT16 and 5DSA added to the reaction mixture are found in the region of the surfactant molecules in the final MCM-41 product, and that the nitroxide spin-label is located near the organic−inorganic interface.[15,16] Here, ^2H

modulation from surfactant molecules labeled at the α-position and ^{14}N modulation from the surfactant headgroup were used to probe changes in the packing of the surfactant molecules around the spin-probe, as illustrated schematically in Figure 1. In addition, changes in the water content of interface region were monitored through the ^{2}H modulation of D_2O in a reaction carried out in D_2O rather than H_2O.

Experimental Section

The reagents used for the synthesis were tetraethyl-orthosilicon (TEOS, Aldrich 98%), cetyltrimethylammonium bromide (CTAB, Aldrich), and NaOH (2N solution). The spin-probes CAT16 and 5DSA were purchased from Molecular Probe Europe BV Company. α-d_2-CTAB was synthesized as described in the literature.[5] All compounds were used without further purification.

MCM-41 containing spin-probes was prepared according to the procedure published earlier[15,16] and the final product was characterized by XRD. In the time evolution experiments, samples were taken from the reaction mixture (at room temperature) at different reaction times and placed into Teflon EPR tubes. Each tube was then immediately inserted into liquid nitrogen, quenching the reaction, and the samples were kept in liquid nitrogen until the ESEEM measurements were performed. It was then quickly transferred into the pre-cooled EPR probehead such that the sample remained frozen. The reference CTAB solutions were prepared by dissolving CTAB and the spin-probe in 3 mL volumetric flasks under stirring and mild heating until homogeneous solutions were obtained. These samples were frozen as described above. In all samples the spin probe concentration was 0.26 mM.

ESEEM experiments were carried out on a home-built pulsed EPR spectrometer.[26] The three-pulse sequence ($\pi/2$-τ-$\pi/2$-T-$\pi/2$-echo) with the appropriate phase cycling[27] was employed. The $\pi/2$ pulse length was 20 ns and the measurements were done at 30 K. The modulation depth was determined either from the time domain waveforms or from the integrated intensity of the corresponding Larmor frequency peak in the Fourier transform (FT) ESEEM spectrum, obtained after subtraction of the background decay. When the time domain traces were employed the modulation depth was taken as $k = a/(a + b)$ where $a + b$ is the interpolated echo intensity between the first and second maxima and b is the echo intensity at the first minima (see Figure 5).

Simulations of the ESEEM traces were carried out using a program written in house based on the theory described in ref 28, the nuclear quadrupole interaction is taken into account and the eigenvalues and eigenfunctions are obtained by numerical diagonalization. The modulation arising from several nuclei was calculated using the spherical averaging model where the nuclei's positions are assumed to be uncorrelated.[19] The search for the best fit parameters was done by a least-squares best fit of the time domain traces. The echo decay in the calculated traces was taken into account by high order polynomial multiplication obtained by fitting the decay of the experimental traces. In the simulations the ^{2}H quadrupole coupling constant e^2qQ/h was taken as 0.2 MHz[29] and the asymmetry parameter η was set to zero. To minimize the number of parameters to be fitted we took the hyperfine and quadrupole tensors as coinciding. This is valid since the quadrupole interaction of ^{2}H in small and the effect of the relative orientation on the ESEEM waveforms is insignificant in the case of the simple model used in this work.

Results

Model Systems and Final Products. Prior to the investigation of the temporal evolution of the ESEEM waveform during the reaction, the ESEEM characteristics of 5DSA and CAT16 in different micellar structures and in different M41S phases were examined. Although there have been several reports in the literature showing that the micellar structure is retained upon fast freezing,[25,30,31] we carried out ESEEM measurements on a series of reference CTAB solutions to substantiate this conclusion. Furthermore, these solutions, which consist of spherical or cylindrical micelles, can serve as a model for changes occurring at the micellar curvature during the reaction. The ESEEM waveforms of CTAB/5DSA solutions, with [CTAB] in the range of 3−17.5 wt % are shown in Figure 2A, and the ESEEM spectra obtained after FT showed a peak at the ^{14}N Larmor frequency (see insert in Figure 2A). The ESEEM waveforms were recorded with a τ value which optimizes the ^{14}N modulation and minimizes the protons modulation. Figure 2B shows the explicit dependence of $k(^{14}N)$ as determined from the intensity of the ^{14}N peak in the FT-ESEEM spectra on [CTAB]. $k(^{14}N)$ is approximately constant up to 6% CTAB, then it increases and levels off at 9.5% CTAB.

The echo intensity $V(\tau,T)$ in the three-pulse ESEEM experiment depends on two factors, one determined by the nuclear modulation effect and the other by the echo decay according to $V(\tau,T) = F_{mod}(\tau,T)F_{relax}(\tau,T)$.[19] $F_{relax}(\tau,T)$ is usually governed by the relaxation times, T_2 and T_1, and spectral and instantaneous diffusion,[35] due to electron spin−spin interactions. It can often be described by an exponential function $F_{relax}(\tau,T) = V_o e^{-T/T_d}$, where the τ dependence is ignored as it is a constant in three-pulse ESEEM experiments. By fitting the ESEEM waveforms to an exponential decay, we obtained T_d values that were [CTAB] dependent, similar to $k(^{14}N)$, as shown in Figure 2B. Both curves show an inflection point around 6 wt %, which corresponds to the transition of spherical to cylindrical micelles. This transition was detected previously by NMR, microscopy, rheology, and scattering techniques.[32−34] Hence, these ESEEM results confirm the preservation of the micellar structures upon rapid freezing.

The $k(^{14}N)$ dependence on [CTAB] shows that $k(^{14}N)_{spheric} < k(^{14}N)_{cylinder}$. This is consistent with the expected changes in the critical packing parameter $g = v/la_0$, where v is the volume of the hydrophobic tail, l is the effective length of the surfactant molecule, and a_0 is the effective area of the hydrophilic headgroup. In micelles $g_{spheric} < g_{cylindric}$.[35] An increase in k is caused by either a decrease in the electron−nuclear distance and/or an increase in the number of interacting nuclei at a particular distance. Considering the spin-probe insertion among the surfactant molecules, it is unlikely that the number of surrounding molecules changes significantly upon the spherical → cylindrical transition. Consequently, we attribute the increase in $k(^{14}N)$ to a decrease in distance between neighboring molecules at the interface due to a change in the curvature. The increase in $k(^{14}N)$ is therefore a consequence of a decrease in a_0, thus leading to a larger value of g under the assumption that v and l do not change.

The spherical to cylindrical micelles transition also results in an increase of T_d, indicating that spectral diffusion, caused by spin−spin interactions,[36] decreases with increasing [CTAB]. Since 5DSA is water insoluble and its concentration is constant in all samples, at low [CTAB] concentrations, where the number of micelles is small, the finite probability to find more than one 5DSA molecule in a single micelle increases the average spin−spin interactions. As [CTAB] increases, the number of

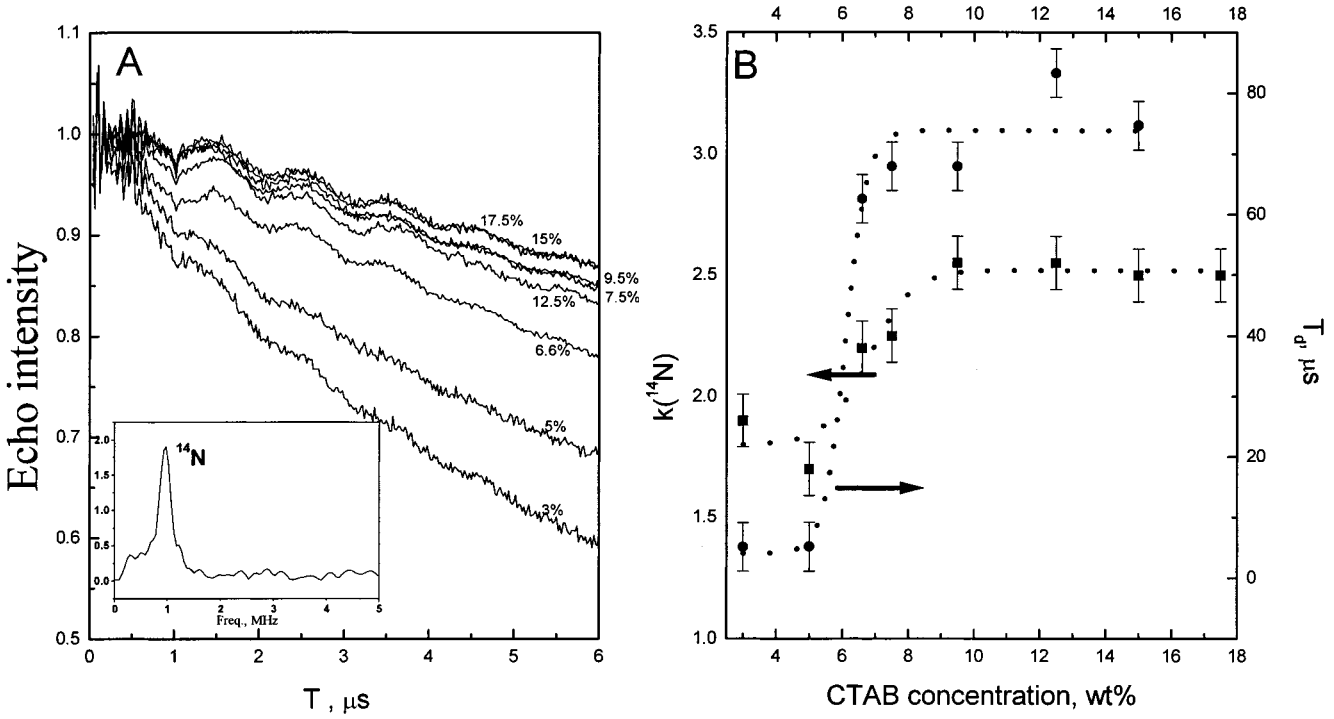

Figure 2. (A) Three-pulse ESEEM traces of 5DSA in various CTAB aqueous solutions as labeled in the figure. (B) Plots of $k(^{14}N)$ (filled squares) and T_d (filled circles) as a function of [CTAB]. $k(^{14}N)$ was determined from the intensity of the ^{14}N peak in the FT-ESEEM spectrum.

micelles increases too, followed by an increase in their size due to the transition to cylindrical micelles. This causes a redistribution of the 5DSA molecules toward a more homogeneous one, increasing their average distance, and reducing the spectral diffusion contribution to the echo decay. The change in T_d also confirms that the micellar structure is conserved upon the freezing.

The dependence of $k(^{14}N)$ on the structure of the final products was also investigated to evaluate its sensitivity to the surfactant curvature at the organic−inorganic interface in the solid. In the case of 5DSA, $k(^{14}N)$ was found to be very shallow and the difference between the various structures was within the noise level. For CAT16, $k(^{14}N)$ was relatively larger, since the nitroxide spin label is closer to the CTAB headgroup and some intramolecular ^{14}N dipolar interactions may also contribute to the modulation depth. $k(^{14}N)$ of CAT16 in MCM-41, MCM-50, and MCM-48, determined from the ESEEM waveforms that were recorded at different magnetic fields along the EPR powder pattern, are presented in Figure 3. The following trend in $k(^{14}N)$ was observed: MCM-50 > MCM-48 > MCM-41.

Under the assumption that $k(^{14}N) \propto g$ (see above), the variation of $k(^{14}N)$ among the different structures is consistent with the predicted trend $g_{lamellar} > g_{cubic} > g_{hexagonal}$ in mesophases.[35] This confirms that the ESEEM results reflect the aggregation behavior of the surfactant molecules in different mesostructures and solutions structures. However, the alternative explanation that the $k(^{14}N)$ trend among the different M41S structures is a result of different conformations or locations of the spin-probe in the different structures cannot be excluded. Nonetheless, this would still reflect a different packing of the surfactant molecules in the three structures.

ESEEM Measurements on the Reaction Mixture. ESEEM experiments on the reaction mixture cannot be performed *in situ*, as is done in CW EPR measurements, because they have to be carried out at low temperatures to slow the echo decay. In addition, since the nuclear modulation arises from anisotropic hyperfine interactions, freezing the molecular motion, that

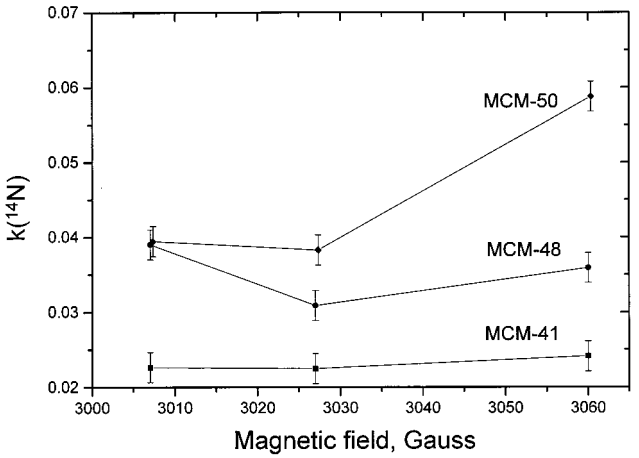

Figure 3. $k(^{14}N)$ of M41S(CAT16) materials measured at different magnetic field along the EPR powder pattern. $k(^{14}N)$ was determined from the time domain traces (see Figure 5).

averages this interaction, is essential. Therefore, the experiments were carried out on samples that were quenched by rapid freezing in liquid nitrogen at different reaction times. The temporal evolution of the local environment of the surfactant molecules near the interface, as manifested by the interaction between the spin-probe and nearby CTAB molecules, can be followed either through ^{14}N modulations or ^{2}H modulation of specifically deuterated α-d_2-CTAB. We have chosen the latter since deeper modulations were observed. In these experiments we favored 5DSA over CAT16 since a fraction of the CAT16 is known to remain in the aqueous solution,[15] outside the micellar assembly, which reduces its sensitivity to the progress of the reaction. Nonetheless, the CAT16 results are presented as supporting evidence.

The time evolution of $k(^{2}H)$ for 5DSA and CAT16 in reactions carried out with α-d_2-CTAB is presented in Figure 4A,B. The dotted line in each graph represents the $k(^{2}H)$ value

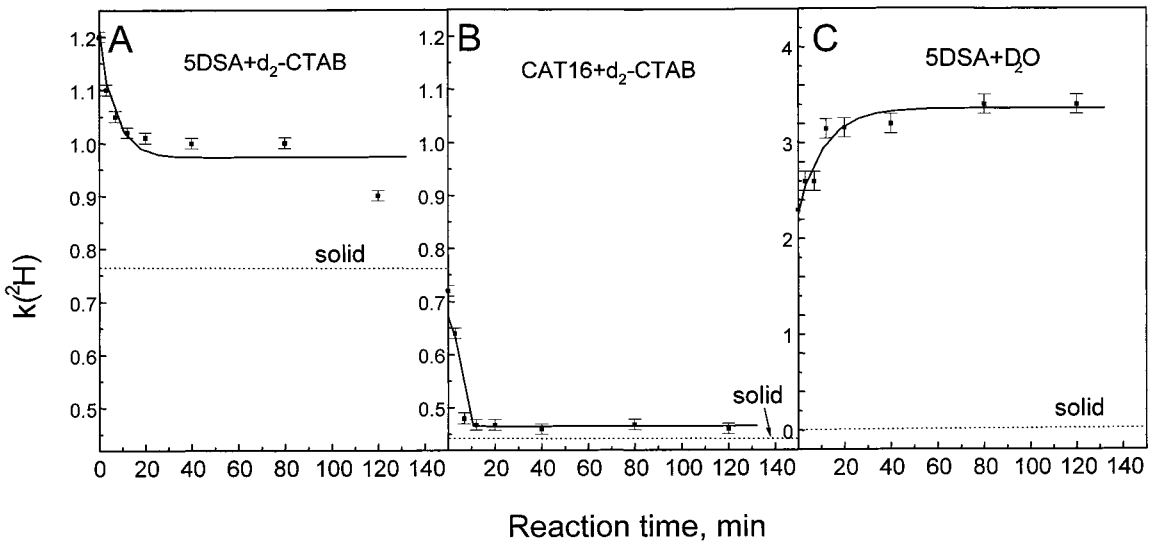

Figure 4. (A) The time evolution of $k(^2H)$ of α-d_2-CTAB for 5DSA during the reaction. (B) Same as (A), but for CAT16. (C) Same as (A) but with normal CTAB and D_2O. The dotted lines represent the $k(^2H)$ values of the corresponding final products. $k(^2H)$ was determined from the intensity of the ^2H peak in the FT-ESEEM spectrum.

of the corresponding final product. A fast initial decrease, lasting about 12 min, followed by leveling off is observed for both spin-probes (Figure 4A,B), although $k(^2H)$ is significantly smaller for CAT16, as expected. This time evolution is similar to that of the phenomenological kinetic curve and the rotational diffusion rates obtained from *in-situ* CW-EPR experiments.[15,16] In both cases, the $k(^2H)$ values of the final products are significantly smaller than those observed from initial reaction mixture. The decrease in $k(^2H)$ indicates a decrease in the distance and/or number of ^2H nuclei in the vicinity of the nitroxide spin-label. To estimate this change we simulated the ESEEM waveforms of the α-d_2-CTAB/5DSA reaction at $t = 0$ (before the addition of TEOS) and after 120 min. We considered a simple model where the modulation is assumed to be induced by an effective number of ^2H nuclei, n_{ef}, at an effective distance, r_{ef}, from the unpaired electron (the NO group of the nitroxide spin label). Figure 5 shows the ESEEM waveforms and the corresponding best fit simulations which for the $t = 0$ trace gave $r_{ef} = 4.48$ Å and $n_{ef} = 1$, whereas for $t = 120$ min $r_{ef} = 4.87$ Å and $n_{ef} = 1$, yielding a difference of 0.4 Å. Although the best fit was obtained with $n_{ef} = 1$ we have carried out additional simulations with a fixed number of nuclei, in the range of 2−5, and fitted r_{ef}. These still showed reasonable agreement with the experimental results, and all revealed a consistent increase in r_{ef} of 0.3−0.4 Å upon increasing t from 0 to 120 min.

While $k(^2H)$ of α-d_2-CTAB decreased during the course of the formation of MCM-41, a reaction mixture with D_2O and normal CTAB showed a small increase of $k(^2H)$ induced by D_2O or OD (Figure 4C). The increase is rapid during the first 12 min and then it levels off, showing the same kinetics as the α-d_2-CTAB/5DSA reaction mixture. Interestingly, no ^2H modulation was observed in the final products with both 5DSA and CAT16, once the solid product was filtered and dried. The ^2H modulation could be restored by soaking the sample in D_2O. We have also attempted to quantify the change in $k(^2H)$ in the D_2O/5DSA synthesis by simulations, but we could not obtain a satisfactory fit with our simple model. The inclusion of a two shell model did not improve the fit significantly. We refrained from building a realistic, complex model of the water or OH distribution since the experimental data available are limited and will not produce a unique answer to a highly complicated

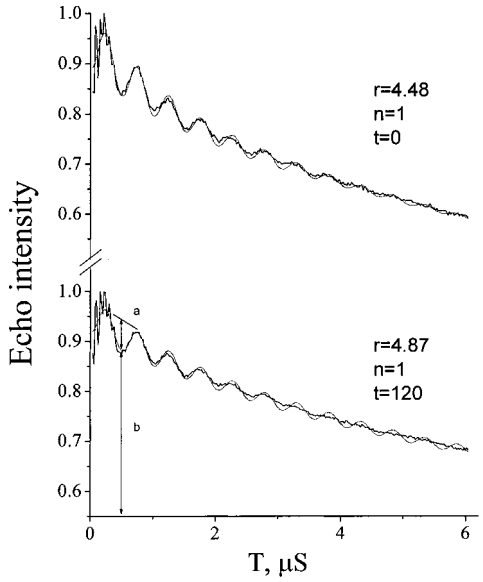

Figure 5. Three-pulse ESEEM waveforms of a α-d_2-CTAB/5DSA reaction and the corresponding simulations (thin solid line) at $t = 0$ (before TEOS addition), simulated with $r_{ef} = 4.48$ Å and $n_{ef} = 1$ and $t = 120$ min and simulation parameters $r_{ef} = 4.87$ Å and $n_{ef} = 1$. In all cases, $\tau = 0.25$ μs and $B_0 = 3014$ G.

situation. Nonetheless, the change in the modulation depth observed during the reaction does show small but significant increase in the density of ^2H around the spin label.

The echo decay time T_d also changes during the reaction, again exhibiting a fast initial increase that levels off at longer times as shown in Figure 6 for 5DSA.

Discussion

The control ESEEM experiments carried out on the CTAB solutions showed that the micellar structure is retained upon fast freezing and that the nuclear modulation effect experienced by both 5DSA and CAT16 is sensitive to the curvature of the interface. This sensitivity was reflected also in the ESEEM measurements on the final MCM-41, -48, and -50 products. The characteristics of the time evolution of $k(^2H)$ during the room-temperature synthesis of MCM-41 in all experiments described

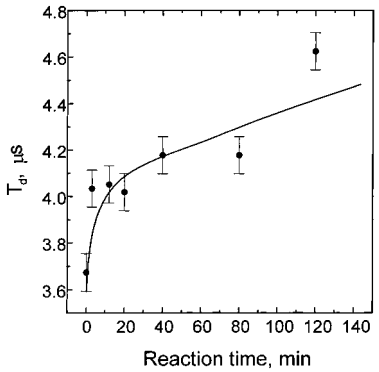

Figure 6. The time evolution of T_d in the α-d_2-CTAB/5DSA reaction.

above is very similar to that of the rotational diffusion rates of 5DSA, which were obtained by room temperature *in-situ* CW-EPR experiments under the same reaction conditions (composition, temperature).[15,16] They exhibit a fast initial process that lasts ∼12 min where the most significant changes take place, followed by a slow process with only subtle changes. This similarity in the kinetics provides additional confirmation that the mesostructures formed during the reaction are not destroyed upon fast freezing.

The small, but significant, increase of $k(^2H)$ of D_2O during the reaction shows that the water (and hydroxyl groups) density in the vicinity of spin-probe molecules increases slightly during the first step of the reaction. Again, this behavior is common for both CAT16 and 5DSA. This suggests that during the first stage, the TEOS hydrolysis forms silicate oligomers that associate at the aggregate interface and create a water rich layer of silicate network. The water content in this newly formed interface is slightly higher than in the original micelles where the counteranions are bromides. According to NMR results, the latter are replaced with multiply charged silicate oligomers during the early stages of the reaction.[5] The existence of a high water content, "soft" silica layer is supported by CW-EPR results that showed that the mobility of 5DSA in a wet as-synthesized product is higher than in the dry product.[16] During the drying process physisorbed water, which comprises the majority of the water, is removed, thus eliminating the D_2O modulation. The process is reversible, namely both the higher mobility of 5DSA and the ^2H modulation are restored upon soaking the sample in D_2O. This is also consistent with the reduction in the *d* spacing (obtained form XRD) by as much as 5 Å, caused by drying room temperature prepared as-synthesized MCM-41 at 100−176 °C.[37] ^{29}Si MAS NMR spectra of the final as-synthesized MCM-41 products (dried at room temperature) that contained different amounts of water exhibited practically the same Q3/Q4, indicating that the degree of the polymerization independent of the water content. Hence, the majority of the water removed upon drying just swells the silicate layer and cross-links domains of silica.

The decrease of $k(^2H)$ of α-d_2-CTAB during the reaction is surprising since an increase in $k(^2H)$ is expected when the packing of the surfactant molecules changes from spherical to cylindrical micelles, as seen from experiments carried out on the CTAB solutions (see Figure 2). A liquid crystalline surfactant-silicate phase was stabilized by the addition of a silicate solution to a low concentration CTAB solution, under conditions that suppress the silicate polymerization.[5] In this case the stability of the hexagonal and lamellar phases formed was attributed to presence of multiply charged silicate anions at the micellar interface. This has two consequences: (i) reduction of the effective Debye length associated with the charge repulsion between aggregates, (ii) reduction of the effective polar-head area due to electrostatic screening caused by the stronger binding of the silicate anions to the surfactant, as compared to the bromides, thus favoring the growth of cylindrical micelles.[5] (In this study the silicate anions have been detected through NMR). Consequently, the average distance at the interface between neighboring surfactant molecules during the MCM-41 formation is expected to decrease, thus leading to an increase in $k(^2H)$. On the basis of the above arguments, the rationale that the decrease in $k(^2H)$ of α-d_2-CTAB arises from an increase in the average distance between surfactant molecules at the interface must be excluded. The reduction in $k(^2H)$ is then associated with a displacement of the spin-probes with respect to the surfactant molecules (see Figure 7). Considering the relative locations of the nitroxide label in the 5DSA molecule and the α-position in CTAB when their polar heads are aligned, a decrease in $k(^2H)$ means a displacement away from the interface toward the organic tails. This displacement is associated with the increasing negative charges at the interface due to binding and polymerization of the silicate anions that leads to a repulsion of the negative polar head of the 5DSA probe toward the inner part of the pore by ∼0.4 Å, as obtained from the simulations. The small displacement of 5DSA toward the organic phase is expected to be associated with a decrease in the water amount in its vicinity, provided there is no change in the water distribution and content at the interface. The experimental results showed a small increase in $k(^2H)$ of D_2O and therefore suggest an increase in the water content of the interface, and maybe, also an increase in the penetration depth into the organic part.

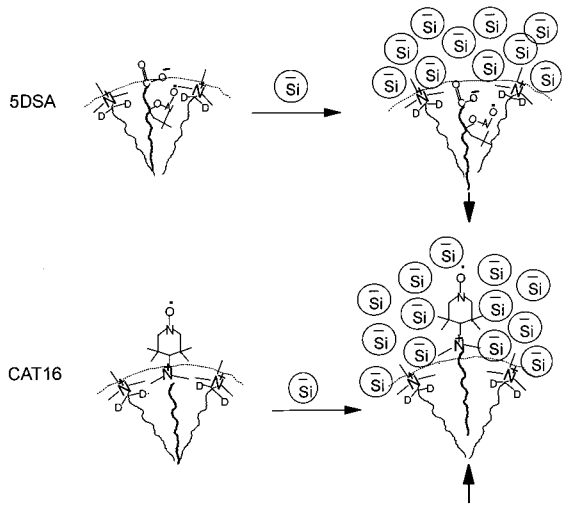

Figure 7. Schematic drawings showing the changes in the location of the spin probes 5DSA and CAT16 within the organic aggregate during the formation of MCM-41. The arrows denote the displacement of the spin-probes.

In contrast to 5DSA, the position of the nitroxide spin label in CAT16 is at the polar head and therefore it is closer to the interface than the α-position of CTAB. Accordingly, the reduction in $k(^2H)$ of α-d_2-CTAB can be explained by an upward displacement, namely protrusion into the silica/water layer (see Figure 7). In this case, the driving force for the protrusion into the silica layer is the steric hindrance of the relatively bulky spin-label at the polar head as a consequence of the reduction in a_0. One other possible explanation for the $k(^2H)$ reduction in CAT16 is an increase in the CAT16 fraction that remains in the water phase during the reaction.[15] This, however, is less likely considering the low $k(^2H)$ in the final product.

The systematic mild increase of T_d during the first step of the reaction suggests that a decrease in the spin−spin interaction

occurs with the progression of the reaction, attributed to a more homogeneous distribution of the spin-probe molecules. Initially, prior to the addition of TEOS, it is likely that more than one spin probe molecules are situated in a micelle thus leading to a substantial dipolar interactions between them, which contributes to spectral diffusion and increases the echo decay. A comparison with the T_d dependence on [CTAB] shows that the change is relatively small (an increase from 3.6 to 4.5 μs, Figure 6, compared to an increase from 1.5 to 80 μs, Figure 2B). The smaller increase is not surprising considering the fact that the surfactant concentration does not increase during the reaction. Nonetheless, this increase shows that there is a rearrangement of the surfactant molecules during the reaction that leads to changes in the distribution of the spin-probes. The increase in the average distances between the spin-probes molecules is consistent with the increase of the size of the aggregates, reducing the probability of finding spin-probes close to each other. The increase in the size of the aggregates is in line with the mechanism proposed by Galarneau et al.[17] who attributed the process of ordering of the solid to a transition from small to larger aggregates.

The process of redistribution of the spin label during the reaction cannot be associated with the contraction of the *d* spacing as reported by *in situ* small angle synchrotron XRD measurements.[10] These measurements were carried out at RT under reaction conditions similar to those employed in this work, with the exception that NH_4OH, rather than NaOH was used as a base. The XRD patterns show that already after 80 s a low angle Bragg diffraction is observed, and that the *d* spacing changes from 46.7 Å after 100 s to 44.9 Å after 500 s. In addition, a change in the relative intensities of the 110/200 reflection has been observed. These results were explained in terms of a model where the hexagonal mesophase initially formed consists of closely packed cylindrical composite aggregates with a circular cross section and with a significant interaggregate space due to electrostatic repulsion. As the polymerization of the silica progresses, interaggregate repulsion decreases, their condensation takes place and the *d* spacing contracts. The contraction of the *d* spacing seems too small to introduce a large enough increase in the dipolar interaction as compared to the decrease attributed to a redistribution of the spin-probes driven by the increased aggregate size combined with the probe's high mobility.

Our results are fully consistent with the notion of silicate oligomers interacting with the surfactant molecules polar-head, but they cannot unambiguously determine whether this occurs at the surface of the original micelles which changed form, as implied by the principles of Monnier et al.[6] and the result of Chemlka and co-workers,[5] or alternatively, that the original micelles are destroyed and the surfactant interacts with formed silicate polymers to yield new structures as suggested by Zana and co-workers.[7,8] Moreover, although we do observe a rearrangement of the spin-probe distribution in the sample, we could not detect directly the spherical to cylindrical micelle transition. This may have occurred before our first experimental time point.

Conclusions

It has been demonstrated that the ESEEM technique is an effective tool for probing changes in the local environment of surfactant-like spin-probes during the formation of MCM-41. Quenching the reaction by rapid cooling to 77 K preserves the micellar structure and therefore allows for low temperature ESEEM measurements. Two stages were detected: the first, during which most changes occur, lasts about 12 min, and is followed by a longer stage with very mild changes. The latter are attributed to further silicate condensation. Experiments carried out with specifically deuterated surfactant molecules revealed that during the first stage $k(^2H)$ of α-d_2-CTAB decreased for 5DSA and CAT16. For 5DSA it was explained in terms of a displacement away from the interface toward the organic core, driven by charge repulsion. For CAT16, in was attributed to an upward displacement, and protrusion into the soft silica layer driven by steric hindrance. The density of water and OH groups in the vicinity of the spin-probe increases slightly at the early stages of the reaction and the forming silica layer has a high water content. The majority of the water is, however, easily removed just by filtering the solid and drying at room temperature. Finally, evidence for the rearrangement of surfactant molecules and the increase in the aggregate size during the first stage of the reaction was deduced from changes in the echo decay time.

Acknowledgment. This work is supported by a grant from the Israeli Ministry of Science and Technology and the Minerva Foundation, Germany.

References and Notes

(1) Beck, J. S.; Vartuli, J. C.; Roth, W. J.; Leonowicz, M. E.; Kresege, C. T.; Schmitt, K. D.; Chu, C. T. W.; Olson, D. H.; Shepard, E. W.; McCullen, S. B.; Higgins, J. B.; Schlenker, J. L. *J. Am. Chem. Soc.* **1992**, *114*, 10834−10843.

(2) Schüth, F. *Studies in Surface Science and Catalysis*; Galarneau, A., Di Renzo, F., Fajula, F., Vedrin, J., Eds.; Elsevier Science B. V.: New York, 2001; Vol. 135, pp 1−12.

(3) Ying, J. Y.; Mehnert, C. P.; Wong, M. S. *Angew. Chem. Int. Ed.* **1999**, *38*, 56−77.

(4) Firouzi, A.; Kumar, D.; Bull, L. M.; Besier, T.; Sieger, P.; Huo, Q.; Walker, S. A.; Zasadzinski, J. A.; Glinka, C.; Nicol, J.; Margolese, D. I.; Stucky, G. D.; Chmelka, B. F. *Science* **1995**, *267*, 1138−1143.

(5) Firouzi, A.; Atef, F.; Oertli, A. G.; Stucky, G. D.; Chmelka, B. F. *J. Am. Chem. Soc.* **1997**, *119*, 3596−3610.

(6) Monnier, A.; Schüth, F.; Huo, Q.; Kumar, D.; Margolese, D.; Maxwell, R. S.; Stucky, G. D.; Krishamurty, M.; Petroff, P.; Firouzi, A.; Janicke, M.; Chmelka, B. F. *Science* **1993**, *261*, 1299−1303.

(7) Zana, R.; Frasch, J.; Soulard, M.; Lebeau, B.; Patarin, J. *Langmuir* **1999**, *15*, 2603−2606.

(8) Sicard, L.; Frasch, J.; Soulard, M.; Lebeau, B.; Patarin, J.; Davey, T.; Zana, R.; Kolenda, F. *Microporous Mesoporous Mat*er. **2001**, 44−45, 25−31.

(9) (a) Linden, M.; Schunk, S.; Schüth, F. In *Mesporous Molecular Sieves, Studies in Surface and Catalysis*; Bonneviot, L., Beland, F., Danumah, C., Giasson, S., Kaliaguine, S., Eds.; Elsevier Science B. V: New York, 1998; Vol. 117, pp 45−52. (b) Linden, M.; Schunk, S.; Schüth, F. *Angew. Chem., Int. Ed. Engl*. **1998**, *37*, 821−823.

(10) Årgen, P.; Lindén, M.; Rosenholm, J. B.; Schwarzenbacher, R.; Kriechbaum, M.; Amenitsch, H.; Laggner, P.; Blanchard, J.; Schüth, F. *J. Phys. Chem. B* **1999**, *103*, 5943−5948.

(11) Calabro, D. C.; Valyocsik, E. W.; Ryan, F. X. *Microporous Mater.* **1996**, *7*, 243−259.

(12) Brown, A. S.; Holt, S. A.; Dam, T.; Trau, M.; White, J. W. *Langmuir* **1997**, *13*, 6363−6365.

(13) Holt, S. A.; Foran, G. F.; White, J. W. *Langmuir* **1999**, *15*, 2540−2542.

(14) Lin, H. P.; Kao, C. P.; Mou, C. Y.; Liu S. B. *J. Phys. Chem. B* **2000**, *104*, 7885−7894.

(15) Zhang, J.; Luz, Z.; Goldfarb, D. *J. Phys. Chem. B* **1997**, *101*, 7087−7094.

(16) Zhang, J.; Luz, Z.; Zimmermann, H.; Goldfarb, D. *J. Phys. Chem.* B **2000**, *104*, 279−285.

(17) Galarneau, A.; Renzo, F.; Fajula, F.; Mollo, L.; Fubini, B.; Ottaviani, M. F. *J. Colloid Interface. Sci.* **1998**, *201*, 105−117.

(18) Regev, O. *Langmuir* **1996**, *12*, 4940−4944.

(19) Kevan, L.; Schwartz, R. N. *Time Domain Electron Spin Resonance* Wiley-Interscience: New York, 1979; Chaper 8.

(20) Deligiannakis, Y.; Louloudi, M.; Hadjiliadis, N. *Coord. Chem. Rev.* **2000**, *204*, 1−122.

(21) Kang, Y. S.; Kevan L. *J. Phys. Chem.* **1994**, *98*, 4389−4392.

(22) Stenland, C.; Kevan, L. *Langmuir* **1994**, *10*, 1129−1133.

(23) Kurshev, V. V.; Kevan L. *J. Phys. Chem.* **1995**, 10616−10620.

(24) Baglioni, P.; Kevan, L. *J. Phys. Chem.* **1987**, *91*, 1516−1518.

(25) Hiff, T.; Kevan, L. *J. Phys. Chem.* **1989**, *93*, 1572−1575.
(26) Shane, J. J.; Gromov, I.; Vega, S.; Goldfarb, D. *Rev. Sci. Instrum.* **1998**, *69*, 3357−3364.
(27) Fauth, J. M.; Schweiger, A.; Braunschweiler, L.; Forrer, J.; Ernst R. R. *J. Magn. Reson.* **1986**, *66*, 74−85.
(28) Goldfarb, D.; Fauth, J. M.; Tor, Y.; Shanzer, A. *J. Am. Chem. Soc.* **1991**, *113*, 1941−1948.
(29) Weiss, A.; Weiden, N. *Advances in Nuclear Quadrupole Resonance*; Smith, J. A. S., Ed.; Heyden: London, 1980; Vol. 4, pp 149−237.
(30) Narayana, P. A.; Li, A. S. W.; Kevan, L. *J. Am. Chem. Soc.* **1981**, *103*, 3603−3604.
(31) Hashimoto, S.; Thomas, J. K. J. *Am. Chem. Soc.* **1983**, *105*, 5230−5327.
(32) Auray, X.; Petipas, C.; Anthore, R.; Rico, L.; Lattes, A. *J. Phys. Chem.* **1989**, *93*, 7458−7464.
(33) Tornblom, M.; Henriksson, U.; Ginley, M. *J. Phys. Chem.* **1994**, *98*, 7041−7051.
(34) Clausen, T. M.; Vinson, P. K.; Minter, J. R.; Davis, H. T.; Talmon, Y.; Miller, W. G. *J. Phys. Chem.* **1992**, *96*, 474−484.
(35) Israelchvili, J.; Mitchell, D. J.; Ninham, B. *Intermolecular and Surfaces Forces*; Academic Press: New York, 1985; pp 1540.
(36) Romanelli, M.; Kevan, L. *Concepts Magn. Reson*. **1997**, *19*, 403−430.
(37) Unpublished results.